International Journal of Mechanical, Industrial and Aerospace Sciences
ISSN: 2517-9950
Vol:3, No:9, 2009

Internal Loading Distribution in Statically Loaded Ball Bearings, Subjected to a Combined Radial and Thrust Load, Including the Effects of Temperature and Fit

Mário C. Ricci

***Abstract*—**A *new*, rapidly convergent, numerical procedure for internal loading distribution computation in statically loaded, single-row, angular-contact ball bearings, subjected to a known combined radial and thrust load, which must be applied so that to avoid tilting between inner and outer rings, is used to find the load distribution differences between a loaded unfitted bearing at room temperature, and the same loaded bearing with interference fits that might experience radial temperature gradients between inner and outer rings. For each step of the procedure it is required the iterative solution of $Z + 2$ simultaneous nonlinear equations – where Z is the number of the balls – to yield exact solution for axial and radial deflections, and contact angles.

***Keywords*—**Ball, Bearing, Static, Load, Iterative, Numerical, Method, Temperature, Fit.

I. Introduction

BALL and roller bearings, generically called *rolling bearings*, are commonly used machine elements. They are employed to permit rotary motions of, or about, shafts in simple commercial devices such as bicycles, roller skates, and electric motors. They are also used in complex engineering mechanisms such as aircraft gas turbines, rolling mils, dental drills, gyroscopes, and power transmissions.

The standardized forms of ball or roller bearings permit rotary motion between two machine elements and always include a complement of ball or rollers that maintain the shaft and a usually stationary supporting structure, frequently called a *housing*, in a radially or axially spaced-apart relationship. Usually, a bearing may be obtained as a unit, which includes two steel rings each of which has a hardened raceway on which hardened balls or rollers roll. The balls or rollers, also called *rolling elements*, are usually held in an angularly spaced relationship by a *cage*, also called a *separator* or *retainer*.

There are many different kinds of rolling bearings. This work is concerned with *single-row angular-contact ball bearings* (Fig. 1) that are designed to support combined radial and thrust loads or heavy thrust loads depending on the *contact angle* magnitude. The bearings having large contact angle can support heavier thrust loads. Fig. 1 shows bearings having small and large contact angles. The bearings generally have groove curvature radii in the range of 52-53% of the ball diameter. The contact angle does not usually exceed 40°.

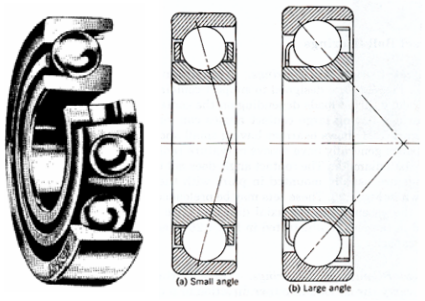

Fig. 1 Angular-contact ball bearing

This work is devoted to study of the internal loading distribution in statically loaded ball bearings. Several researchers have studied the subject as, for example, Stribeck [1], Sjoväll [2], Jones [3] and Rumbarger [4]. The methods developed by them to calculate distribution of load among the balls and rollers of rolling bearings can be used in most bearing applications because rotational speeds are usually slow to moderate. Under these speed conditions, the effects of rolling element centrifugal forces and gyroscopic moments are negligible. At high speeds of rotation these body forces become significant, tending to alter contact angles and clearance. Thus, they can affect the static load distribution to a great extension.

Harris [5] described methods for internal loading distribution in statically loaded bearings addressing pure radial; pure thrust (centric and eccentric loads); combined radial and thrust load, which uses radial and thrust integrals introduced by Sjoväll; and for ball bearings under combined radial, thrust, and moment load, initially due to Jones.

There are many works describing the parameters variation

M. C. Ricci is with the Brazilian Institute for Space Research, São José dos Campos, 12227-010 Brazil (e-mail: mariocesarricci@uol.com.br).

M. C. Ricci thanks the financial support provided by the Brazilian Institute for Space Research (INPE), the Brazilian Scientific and Technological Development Council (CNPq), and The State of São Paulo Research (FAPESP).

models under static loads but few demonstrate such variations in practice, even under simple static loadings. The author believes that the lack of practical examples is mainly due to the inherent difficulties of the numerical procedures that, in general, deal with the resolution of several non-linear algebraic equations that must to be solved simultaneously.

In an attempt to cover this gap studies are being developed in parallel [6], [7], [8]. Particularly in this work a new, precise numerical procedure, described in [7], for internal load distribution computation in statically loaded, single-row, angular-contact ball bearings subjected to a known external combined radial and thrust load, so that no tilt is allowed between inner and outer rings, is used to find the load distribution differences between a loaded bearing with clearance fits at room temperature, and the same loaded bearing with interference fits, such might experience radial temperature gradients between inner and outer rings.

In the most usual situation, angular contact bearings would first be fitted, with interference or clearance defined at room temperature, to their respective shaft and housing; then a defined axial "hard" preload would be applied and subsequently in operation the bearings might experience radial temperature gradients between inner and outer rings.

Generally, ball bearings and other radial rolling bearings such as cylindrical roller bearings are designed to have a diametral clearance in the no-load state. Due to this radial clearance the bearing also can experience an axial play. Removal of this axial freedom causes the ball-raceway contact line to assume an oblique angle with respect to the radial plane; hence, a contact angle different from zero will occur. This angle is called *free contact angle* and is a function of clearance built into the unloaded bearing and the raceway groove curvatures.

Press or shrink fitting of the inner ring on the shaft causes the inner ring to expand slightly. Similarly, press fitting of the outer ring in the housing causes the former member to shrink slightly. Thus, the bearing's diametral clearance will tend to decrease. Large amounts of interference in fitting practice can cause bearing clearance to vanish and even produce negative clearance or interference in the bearing.

Thermal conditions of bearing operation can also affect the diametral clearance. Heat generated by friction causes internal temperatures to rise. This in turn causes expansion of the shaft, housing, and bearing components. Depending on the shaft and housing materials and on the magnitude of thermal gradients across the bearing and these supporting structures, clearance can tend to increase or decrease. It is also apparent that the thermal environment in which a bearing operates may have a significant effect on clearance.

II. Symbols

a Semimajor axis of the projected contact, m
A Distance between raceway groove curvature centers, m
b Semiminor axis of the projected contact, m
B $f_o + f_i - 1$, total curvature
d Raceway diameter, m
d_a Bearing outer diameter, m
d_b Bearing inner diameter, m
d_e Bearing pitch diameter, m
d_1 Housing outside diameter, m
d_2 Shaft hole diameter, m
D Ball diameter, m
E Modulus of elasticity, N/m^2
E' Effective elastic modulus, N/m^2
$\mathbf{E}$ Elliptic integral of second kind
f Raceway groove radius ÷ D
F Applied load, N
I Diametral interference, m
k a/b
K Load-deflection factor, N/m$^{3/2}$
$\mathbf{K}$ Elliptic integral of first kind
M Sum of the ball loads moments about inner ring center of mass, Nm
P_d Diametral clearance, m
P_e Free endplay, m
Q Ball-raceway normal load, N
r Raceway groove curvature radius; solids curvature radius, m
s Distance between loci of inner and outer raceway groove curvature centers, m
R Curvature radius; radius of locus of raceway groove curvature centers, m
T Temperature, ^{o}C
Z Number of rolling elements
β Contact angle, rad, ^{o}
β_f Free contact angle, rad, ^{o}
γ $D \cos \beta / d_e$
Γ Curvature difference or coefficient of linear expansion, m/m/^{o}C
δ Deflection or contact deformation, m
Δ Variation or Clearance reduction due to press fitting, m
$\Delta\psi$ Angular spacing between rolling elements, rad,^{o}
υ Poisson's ratio
φ Auxiliary angle
ψ Azimuth angle, rad, ^{o}

Subscripts:

a Refers to solid a, axial direction or ambient temperature
b Refers to solid b or bearing
x,y Refers to coordinate system
h Refers to housing
i Refers to inner raceway
j Refers to rolling element position
n Refers to direction collinear with normal load; integer number
o Refers to outer raceway
r Refers to radial direction
s Refers to shaft

III. Geometry of Ball Bearings

In this section, the principal geometrical relationships for an unloaded ball bearing are summarized. The radial cross section of a single-row ball bearing shown in Fig. 2 depicts the *diametral clearance* and various diameters. The *pitch diameter*, d_e, is the mean of the inner- and outer-race diameters, d_i and d_o, respectively, and is given by

$$d_e = \frac{1}{2}(d_i + d_o). \quad (1)$$

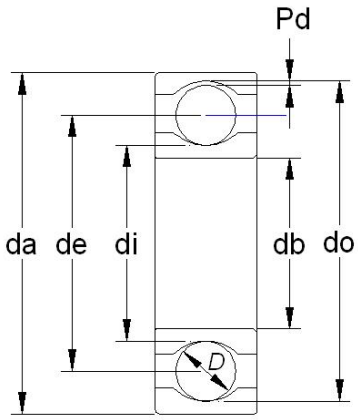

Fig. 2 Radial cross section of a single-row ball bearing

The diametral clearance, P_d, can be written as

$$P_d = d_o - d_i - 2D. \quad (2)$$

Race conformity is a measure of the geometrical conformity of the race and the ball in a plane passing through the bearing axis (also named center line or rotation axis), which is a line passing through the center of the bearing perpendicular to its plane and transverse to the race. Fig. 3 depicts a cross section of a ball bearing showing race conformity, expressed as

$$f = r/D. \quad (3)$$

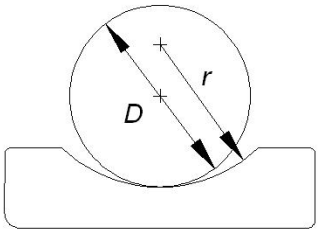

Fig. 3 Cross section of a ball and an outer race showing race conformity

Radial bearings have some axial play since they are generally designed to have a diametral clearance, as shown in Fig. 4(a). Fig. 4(b) shows a radial bearing with contact due to the axial shift of the inner and outer rings when no measurable force is applied. The radial distance between the curvature centers of the two races are the same in the Figs. 4(a) and (b). Denoting quantities referred to the inner and outer races by subscripts *i* and *o*, respectively, this radial distance value can be expressed as $A - P_d/2$, where $A = r_o + r_i - D$ is the curvature centers distance in the shifted position given by Fig. 4(b). Using (3) we can write A as

$$A = BD, \quad (4)$$

where $B = f_o + f_i - 1$ is known as the *total conformity ratio* and is a measure of the combined conformity of both the outer and inner races to the ball.

The *contact angle*, β, is defined as the angle made by a line, which passes through the curvature centers of both the outer and inner raceways and that lies in a plane passing through the bearing rotation axis, with a plane perpendicular to the bearing axis of rotation. The *free-contact angle*, β_f, (Fig. 4(b)) is the contact angle when the line also passes through the points of contact of the ball and both raceways and no measurable force is applied. From Fig. 4(b), the expression for the free-contact angle can be written as

$$\cos\beta_f = \frac{A - P_d/2}{A}. \quad (5)$$

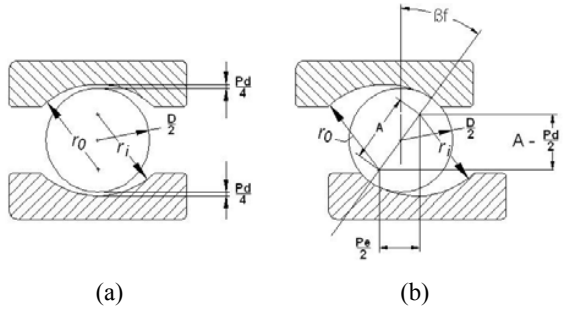

(a) (b)

Fig. 4 Cross section of a radial ball bearing showing ball-race contact due to axial shift of inner and outer rings. (a) Initial position. (b) Shifted position

From (5), the diametral clearance, P_d, can be written as

$$P_d = 2A(1 - \cos\beta_f). \quad (6)$$

Free endplay, P_e, is the maximum axial movement of the inner race with respect to the outer when both races are coaxially centered and no measurable force is applied. Free endplay depends on total curvature and contact angle, as shown in Fig. 4(b), and can be written as

$$P_e = 2A\sin\beta_f. \quad (7)$$

Considering the geometry of two contacting solids (ellipsoids *a* and *b*) in a ball bearing we can arrive at the two quantities of some importance in the analysis of contact stresses and deformations: The curvature sum, $1/R$, and curvature difference, Γ, which are defined as:

$$\frac{1}{R}=\frac{1}{R_x}+\frac{1}{R_y},$$
$$\Gamma = R\left(\frac{1}{R_x}-\frac{1}{R_y}\right),$$

where

$$\frac{1}{R_x}=\frac{1}{r_{ax}}+\frac{1}{r_{bx}},$$
$$\frac{1}{R_y}=\frac{1}{r_{ay}}+\frac{1}{r_{by}},$$

with r_{ax}, r_{bx}, r_{ay} and r_{by}, being the radii of curvature for the ball-race contact.

A cross section of a ball bearing operating at a contact angle β is shown in Fig. 5. Equivalent radii of curvature for both inner- and outer-race contacts in, and normal to, the direction of rolling can be calculated from this figure. Considering x the direction of the motion and y the transverse direction, the radii of curvature for the ball-inner-race contact are

$$r_{ax}=r_{ay}=D/2,$$
$$r_{bx}=\frac{d_e-D\cos\beta}{2\cos\beta},$$
$$r_{by}=-f_iD=-r_i.$$

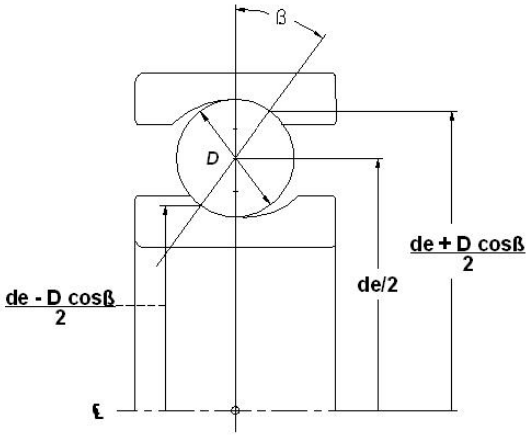

Fig. 5 Cross section of a ball bearing

The radii of curvature for the ball-outer-race contact are

$$r_{ax}=r_{ay}=D/2,$$
$$r_{bx}=\frac{d_e+D\cos\beta}{2\cos\beta},$$
$$r_{by}=-f_oD=-r_o.$$

Let

$$\gamma=\frac{D\cos\beta}{d_e}.$$

Then

$$r_{bx}=\frac{D}{2}\frac{1-\gamma}{\gamma},$$
$$\left.\frac{1}{R}\right|_i=\frac{1}{r_{ax}}+\frac{1}{r_{bx}}+\frac{1}{r_{ay}}+\frac{1}{r_{by}}=\frac{1}{D}\left(4-\frac{1}{f_i}+\frac{2\gamma}{1-\gamma}\right), \quad (8)$$
$$\Gamma_i=R\left(\frac{1}{r_{ax}}+\frac{1}{r_{bx}}-\frac{1}{r_{ay}}-\frac{1}{r_{by}}\right)=\frac{\frac{1}{f_i}+\frac{2\gamma}{1-\gamma}}{4-\frac{1}{f_i}+\frac{2\gamma}{1-\gamma}}, \quad (9)$$

for the ball-inner-race contact, and

$$r_{bx}=-\frac{D}{2}\frac{1+\gamma}{\gamma},$$
$$\left.\frac{1}{R}\right|_o=\frac{1}{r_{ax}}+\frac{1}{r_{bx}}+\frac{1}{r_{ay}}+\frac{1}{r_{by}}=\frac{1}{D}\left(4-\frac{1}{f_o}-\frac{2\gamma}{1+\gamma}\right), \quad (10)$$
$$\Gamma_o=R\left(\frac{1}{r_{ax}}+\frac{1}{r_{bx}}-\frac{1}{r_{ay}}-\frac{1}{r_{by}}\right)=\frac{\frac{1}{f_o}-\frac{2\gamma}{1+\gamma}}{4-\frac{1}{f_o}-\frac{2\gamma}{1+\gamma}}, \quad (11)$$

for the ball-outer-race contact.

IV. Effects of Interference Fitting, Thermal Gradients, and Surface Finish on Clearance

In this section, the principal relationships between interference fittings, thermal gradients, surface finish and changes in diametral clearance are summarized. As described in [5], the increase in d_i due a press fitting between a bearing inner ring and a shaft of hole diameter d_2, is given by

$$\Delta_s=\frac{2Id_i/d_b}{\left[(d_i/d_b)^2-1\right]\left\{\frac{(d_i/d_b)^2+1}{(d_i/d_b)^2-1}+\nu_b+\frac{E_b}{E_s}\left[\frac{(d_b/d_2)^2+1}{(d_b/d_2)^2-1}-\nu_s\right]\right\}} \quad (12)$$

If the bearing inner ring and shaft are both fabricated from the same material, then

$$\Delta_s=I\frac{d_i}{d_b}\left[\frac{(d_b/d_2)^2-1}{(d_i/d_2)^2-1}\right]. \quad (13)$$

For a bearing inner ring mounted on a solid shaft of the same material, diameter d_2 is zero and

$$\Delta_s=Id_b/d_i. \quad (14)$$

Similarly, the decrease in d_o due a press fitting between a bearing outer ring and a housing of outside diameter d_1, is given by

$$\Delta_h=\frac{2Id_a/d_o}{\left[(d_a/d_o)^2-1\right]\left\{\frac{(d_a/d_o)^2+1}{(d_a/d_o)^2-1}-\nu_b+\frac{E_b}{E_h}\left[\frac{(d_1/d_a)^2+1}{(d_1/d_a)^2-1}+\nu_h\right]\right\}} \quad (15)$$

If the bearing outer ring and housing are both fabricated from the same material, then

$$\Delta_h = I\frac{d_a}{d_o}\left[\frac{(d_1/d_a)^2-1}{(d_1/d_o)^2-1}\right]. \quad (16)$$

For a bearing outer ring mounted inside a solid housing of the same material, diameter d_1 approaches infinity and

$$\Delta_h = Id_o/d_a. \quad (17)$$

A reduction in I due to surface finish must be taking into account [5].

Now, considering bearing outer and inner rings at temperatures $T_o - T_a$ and $T_i - T_a$ above ambient, respectively, the approximate increases in d_o and d_i are $\Gamma_b d_o(T_o - T_a)$ and $\Gamma_b d_i(T_i - T_a)$, respectively. Thus the diametral clearance increase due to thermal expansion is

$$\Delta_T = \Gamma_b d_o(T_o - T_a) + \Gamma_b d_i(T_i - T_a). \quad (18)$$

When the housing and shaft are not fabricated from the same material (usually steel) as the bearing, an increase in the interference can be wait, that are given by $(\Gamma_b - \Gamma_h)d_a(T_o - T_a)$ and $(\Gamma_s - \Gamma_b)d_b(T_i - T_a)$, respectively.

Considering a bearing having a clearance P_d prior to mounting at room temperature, the change in clearance, after mounting with bearing outer and inner rings at temperatures T_o and T_i, respectively, is given by

$$\Delta P_d = \Delta_T - \Delta_s - \Delta_h. \quad (19)$$

V. Contact Stress and Deformations

When two elastic solids are brought together under a load, a contact area develops, the shape and size of which depend on the applied load, the elastic properties of the materials, and the curvatures of the surfaces. For two ellipsoids in contact the shape of the contact area is elliptical, with a being the semi-major axis in the y direction (transverse direction) and b being the semi-minor axis in the x direction (direction of motion).

The *elliptical eccentricity parameter*, k, is defined as?

$$k = a/b.$$

From [5], k can be written in terms of the curvature difference, Γ, and the *elliptical integrals of the first and second kind*, **K** and **E**, as

$$J(k) = \sqrt{\frac{2\mathbf{K} - \mathbf{E}(1+\Gamma)}{\mathbf{E}(1-\Gamma)}},$$

where

$$\mathbf{K} = \int_0^{\pi/2}\left[1-\left(1-\frac{1}{k^2}\right)\sin^2\varphi\right]^{-1/2} d\varphi,$$

$$\mathbf{E} = \int_0^{\pi/2}\left[1-\left(1-\frac{1}{k^2}\right)\sin^2\varphi\right]^{1/2} d\varphi.$$

A one-point iteration method, which has been used successfully in the past [9], is used here, where

$$k_{n+1} = J(k_n).$$

When the *ellipticity parameter*, k, the *elliptic integrals of the first* and *second kinds*, **K** and **E**, respectively, the normal applied load, Q, Poisson's ratio, v, and the modulus of elasticity, E, of the contacting solids are known, we can write the semi-major and -minor axes of the contact ellipse and the maximum deformation at the center of the contact, from the analysis of Hertz [10], as

$$a = \left(\frac{6k^2\mathbf{E}QR}{\pi E'}\right)^{1/3}, \quad (20)$$

$$b = \left(\frac{6\mathbf{E}QR}{\pi k E'}\right)^{1/3}, \quad (21)$$

$$\delta = \mathbf{K}\left[\frac{9}{2\mathbf{E}R}\left(\frac{Q}{\pi k E'}\right)^2\right]^{1/3}, \quad (22)$$

where

$$E' = \frac{2}{\frac{1-\upsilon_a^2}{E_a} + \frac{1-\upsilon_b^2}{E_b}}.$$

VI. Static Load Distribution Under Combined Radial and Thrust Load

Methods to calculate distribution of load among the balls and rollers of rolling bearings statically loaded can be found in various papers, [11]. The methods have been limited to, at most, three degrees of freedom in loading and demand the solution of a simultaneous nonlinear system of algebraic equations for higher degrees of freedom. Solution of such equations generally necessitates the use of a digital computer. In certain cases, however – for example, applications with pure radial, pure thrust or radial and thrust loading with nominal clearance – the simplified methods will probably provide sufficiently accurate calculational results.

Having defined a simple analytical expression for the deformation in terms of load in the previous section, it is possible to consider how the bearing load is distributed among the rolling elements. Most rolling-element bearing applications involve steady-state rotation of either the inner or outer race or both; however, the speeds of rotation are usually not so great as to cause ball or roller centrifugal forces or gyroscopic moments of significant magnitudes. In analyzing the loading distribution on the rolling elements, it is usually

satisfactory to ignore these effects in most applications. In this section the load deflection relationships for ball bearings are given, along with a specific load distribution consisting of a combined radial and thrust load, which must be applied to the inner ring of a statically loaded ball bearing, so that no tilt is allowed between inner and outer rings.

A. Load-Deflection Relationships for Ball Bearings

From (22) it can be seen that for a given ball-raceway contact (point loading)

$$Q = K\delta^{3/2}, \tag{23}$$

where

$$K = \pi k E' \sqrt{\frac{2\mathbf{E}R}{9\mathbf{K}^3}}.$$

The total normal approach between two raceways under load separated by a rolling element is the sum of the approaches between the rolling element and each raceway. Hence

$$\delta_n = \delta_i + \delta_o.$$

Therefore,

$$K_n = \left[\frac{1}{1/K_i^{2/3} + 1/K_o^{2/3}}\right]^{3/2}$$

and

$$Q = K_n \delta_n^{3/2}. \tag{24}$$

B. Ball Bearings under Combined Radial and Thrust Load

According [7], let a ball bearing with a number of balls, Z, symmetrically distributed about a pitch circle according to Fig. 6, to be subjected to a combined radial and thrust load, so that a *relative axial displacement*, δ_a, and a *relative radial displacement*, δ_r, between the inner and outer ring raceways may be expected. Let $\psi = 0$ to be the angular position of the maximum loaded ball.

Fig. 7 shows the initial and final curvature centers positions at angular position ψ, before and after loading, considering that the centers of curvature of the raceway grooves are fixed with respect to the corresponding raceway. If δ_a and δ_r are known, the contact angle at angular position ψ, after the combined load has been applied, is given by

$$\beta(\psi) = \cos^{-1}\left(\frac{A\cos\beta_f + \delta_r\cos\psi}{A + \delta_n}\right). \tag{25}$$

Also, from Fig. 7,

$$\delta_a(\psi) = (A + \delta_n)\sin\beta - A\sin\beta_f, \tag{26}$$

and we can arrive in the expression for the extend of the *loading zone*, that is given by:

$$\psi_l = \cos^{-1}\left\{\frac{A}{\delta_r}\left[\cos\left(\sin^{-1}\left(\frac{\delta_a + A\sin\beta_f}{A}\right)\right) - \cos\beta_f\right]\right\}. \tag{27}$$

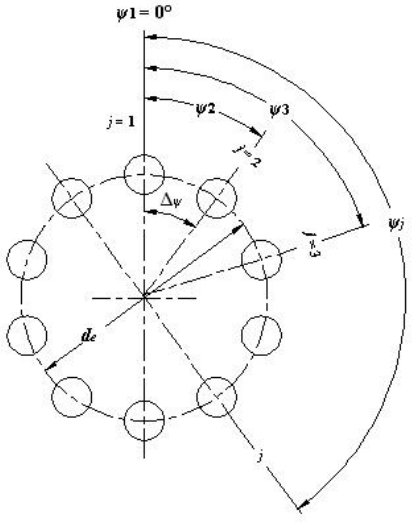

Fig. 6 Ball angular positions in the radial plane that is perpendicular to the bearing's axis of rotation, $\Delta\psi = 2\pi/Z$, $\psi_j = 2\pi/Z(j-1)$

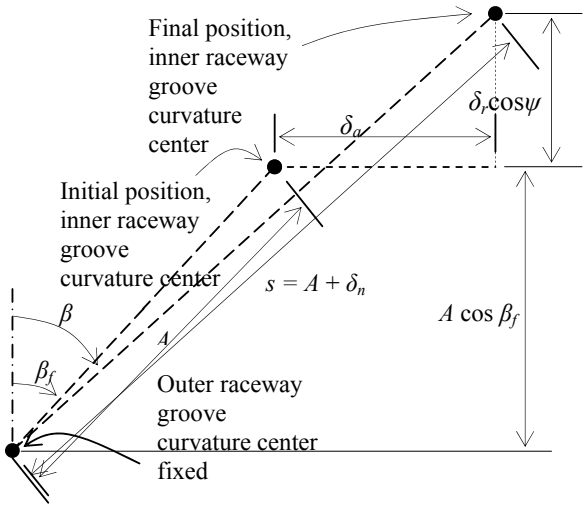

Fig. 7 Initial and final curvature centers positions at angular position ψ, with and without applied load

From (25), the total normal approach between two raceways at angular position ψ, after the combined load has been applied, can be written as

$$\delta_n(\psi) = A\left(\frac{\cos\beta_f}{\cos\beta} - 1\right) + \frac{\delta_r\cos\psi}{\cos\beta}. \tag{28}$$

From Fig. 7 and (28) it can be determined that s, the distance between the centers of the curvature of the inner and outer ring raceway grooves at any rolling element position ψ, is given by:

$$s(\psi) = A + \delta_n = A\frac{\cos\beta_f}{\cos\beta} + \frac{\delta_r \cos\psi}{\cos\beta}. \quad (29)$$

From (26) and (29) yields, for $\psi = \psi_j$,

$$\delta_a - \delta_r \tan\beta_j \cos\psi_j - A\frac{\sin(\beta_j - \beta_f)}{\cos\beta_j} = 0, j = 1,\ldots,Z. \quad (30)$$

From (24) and (28) yields, for $\psi = \psi_j$,

$$Q_j = K_{nj}\left[A\left(\frac{\cos\beta_f}{\cos\beta_j} - 1\right) + \frac{\delta_r \cos\psi_j}{\cos\beta_j}\right]^{3/2}, \; j = 1,\ldots, Z. \quad (31)$$

If a thrust load, F_a, and a radial load, F_r, are applied then, for static equilibrium to exist

$$F_a = \sum_{j=1}^{Z} Q_j \sin\beta_j, \quad (32)$$

$$F_r = \sum_{j=1}^{Z} Q_j \cos\beta_j \cos\psi_j. \quad (33)$$

Additionally, each of the normal ball load components produces a moment about of the inner ring center of mass, in the plan, which passes through the bearing rotation axis and contains the external radial load (moments about the other two perpendicular plans are self-equilibrating). For static equilibrium, the thrust load, F_a, and/or the radial load, F_r, must exert a moment, M, about of the inner ring center of mass, which must be equal the sum of the moments of each rolling element load, that is,

$$M = -\sum_{j=1}^{Z} Q_j \sin\beta_j \left[(R_i + \delta_r \cos\psi_j)\cos\psi_j - \delta_r\right], \quad (34)$$

where

$$R_i = d_e/2 + (f_i - 0.5)D\cos\beta_f$$

expresses the locus of the centers of the inner ring raceway groove curvature radii.

Substitution of (31) into (32) yields

$$F_a - \sum_{j=1}^{Z} K_{nj}\sin\beta_j \left(A\left(\frac{\cos\beta_f}{\cos\beta_j} - 1\right) + \frac{\delta_r \cos\psi_j}{\cos\beta_j}\right)^{3/2} = 0. \quad (35)$$

Similarly,

$$F_r - \sum_{j=1}^{Z} K_{nj}\cos\psi_j \cos\beta_j \left(A\left(\frac{\cos\beta_f}{\cos\beta_j} - 1\right) + \frac{\delta_r \cos\psi_j}{\cos\beta_j}\right)^{3/2} = 0. \quad (36)$$

Equations (30), (35) and (36) are $Z + 2$ simultaneous nonlinear equations with unknowns δ_a, δ_r, and β_j, $j = 1,\ldots, Z$. Since K_{nj} are functions of contact angle, β_j, the equations must be solved iteratively to yield an exact solution for δ_a, δ_r and β_j.

VII. Numerical Results

To show an application of the theory developed in this work a numerical example is presented, which uses the Newton-Rhapson method to solve the simultaneous nonlinear equations (30), (35) and (36).

218 angular-contact ball bearing as example, which was also used by [5] have been chosen. The 218 angular-contact ball bearing has a 0.09 m bore, a 0.16 m o.d. and is manufactured to ABEC 7 tolerance limits. The bearing is mounted on a hollow steel shaft of 0.0635 m bore with a k6 fit and in a titanium housing having a effective o.d. of 0.2032 m with an M6 fit. Considers that the inner ring operates at a mean temperature of 148.9°C, that the outer ring is at 121.1°C and that the bearing was assembled at 21.1°C.

There are three steps in the numerical procedure. The first, considering the bearing unfitted at assembling temperature; the second, considering the fits above at assembling temperature; and the third, considering the fits above at operational temperatures for the inner and outer rings. Before each step the geometry of the bearing is obtained from which, the nonlinear equations are solved simultaneously to obtain radial and axial deflections and contact angles.

Figs. 8 to 17 show some parameters, as functions of the applied thrust load, for the three steps of the procedure and for some values of the applied radial load.

Figs. 8 and 9 show the normal ball loads for the maximum and minimum loaded ball, respectively. There is a better loading distribution with the increase of thrust load; and there are slight decreases (increases) in normal ball load, for the maximum (minimum) loaded ball, when it passes from first to second, and from second to third steps. Similar behavior is also observed for other parameters and will not be mentioned here. For this loading range, the ball at angular position $\psi = 0$ is always loaded. This is not the case for the ball at angular position $\psi = 180°$. For zero applied radial load the normal ball load is the same for the maximum and minimum loaded ball.

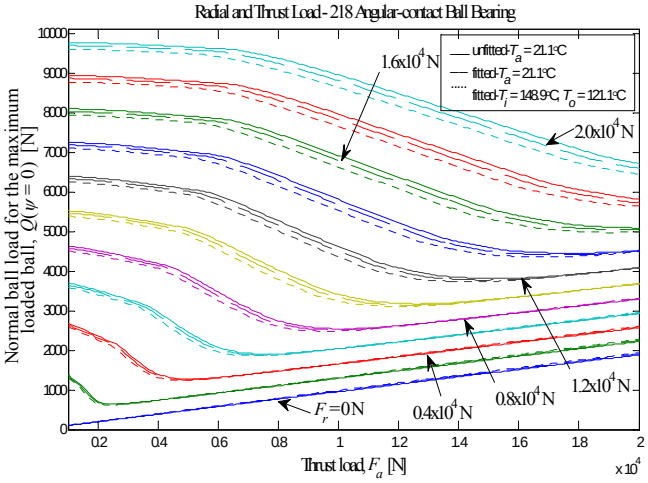

Fig. 8 Normal ball load for the maximum loaded ball, $Q(\psi = 0)$, as a function of the thrust load, F_a

Figs. 10 and 11 show the contact angle for the maximum and minimum loaded ball, respectively. The straight lines represent the free contact angles for the three steps of the procedure. For zero applied radial load the contact angle is always greater than the free contact angle. In this case, the bearing is under thrust loading and all balls have the same load and contact angles. If the contact angle falls below the free contact angle the balls are unloaded. With the increase in applied radial load the free contact angle ceases to be a reference for unload. In this case, the contact angle may drop to values much lower than the free contact angle value - as low as 3° - for a loaded ball, or may rise to values greater than the free contact angle value, for an unloaded ball.

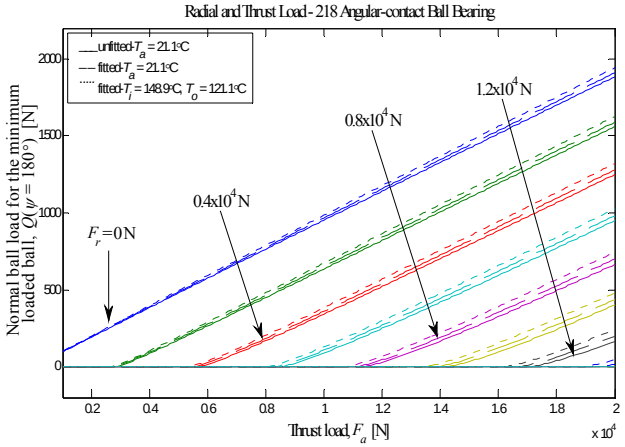

Fig. 9 Normal ball load for the minimum loaded ball, $Q(\psi = 180°)$, as a function of the thrust load, F_a

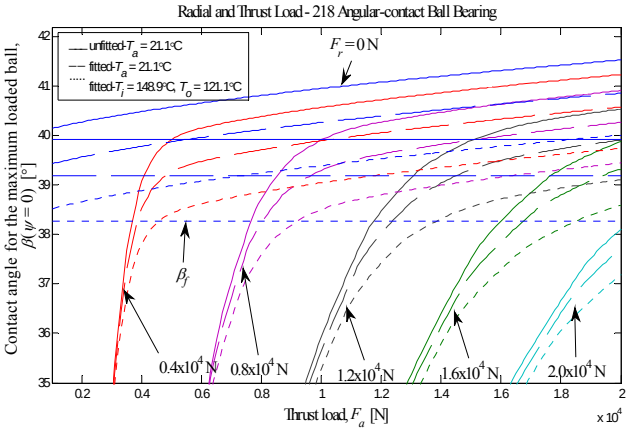

Fig. 10 Contact Angle for the maximum loaded ball, $\beta(\psi = 0)$, as a function of the thrust load, F_a

Figs. 12 and 13 show the distance between the curvature centers for the maximum and minimum loaded ball, s, respectively. The straight lines represent the curvature centers distance in the shifted (unload) position, A. Simply remove A from s for total deformation along the contact line. If s falls below A is an indication of unloading.

Fig. 14 shows the loading zone. The straight lines represent the angular ball positions. With the increase of thrust load there is an increase of the loading angle, whose maximum value is 180°.

Figs. 15 and 16 show the axial and radial deflections, respectively.

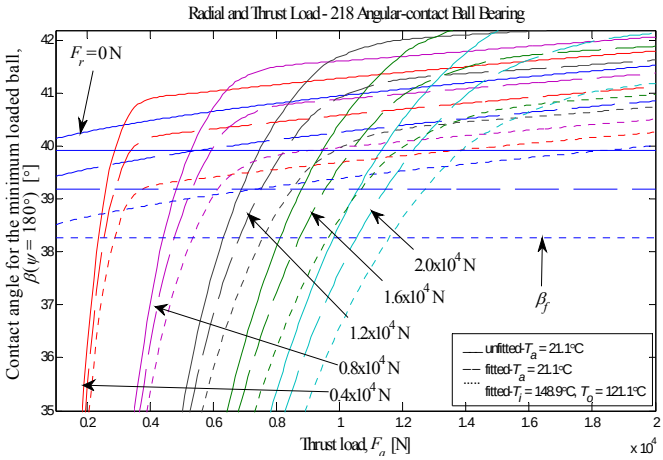

Fig. 11 Contact Angle for the minimum loaded ball, $\beta(\psi = 180°)$, as a function of the thrust load, F_a

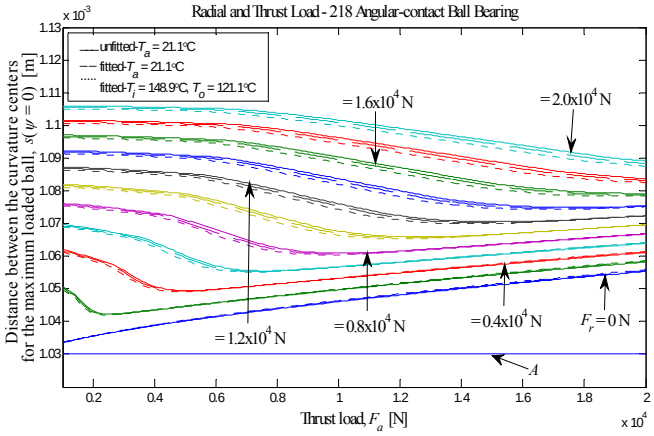

Fig. 12 Distance between the curvature centers for the maximum loaded ball, $s(\psi = 0)$, as a function of the thrust load, F_a

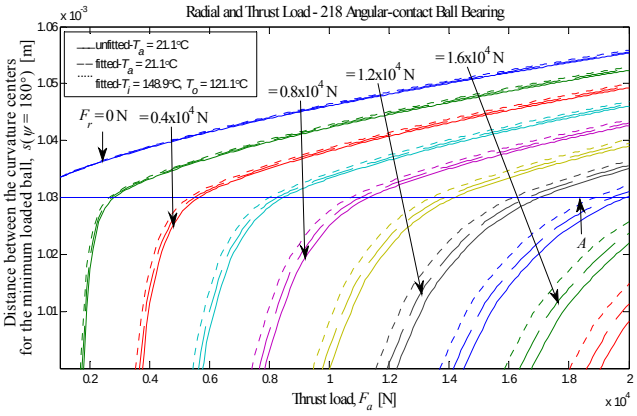

Fig. 13 Distance between the curvature centers for the minimum loaded ball, $s(\psi = 180°)$, as a function of the thrust load, F_a

VIII. Conclusion

The importance of this work lies in the fact that it uses a *new* procedure for get numerically, accurately and quickly, the static load distribution of a ball bearing under axial and radial loading, taking into account the influence of fits and thermal gradients. Precise applications, as for example, space applications, require a precise determination of the static loading. Models available in literature are approximate and often are not compatible with the desired degree of accuracy. This work can be extended to determine the loading on high-speed bearings where centrifugal and gyroscopic forces do not be discarded. The results of this work can be used in the accurate determination of the friction torque of the ball bearings, under any operating condition of temperature and speed.

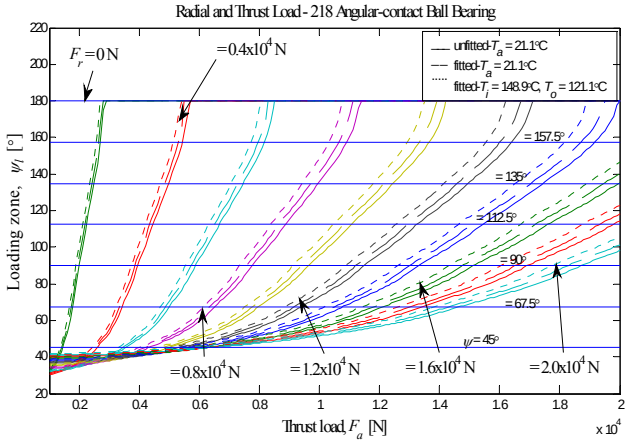

Fig. 14 Loading zone, ψ_l, as a function of the thrust load, F_a

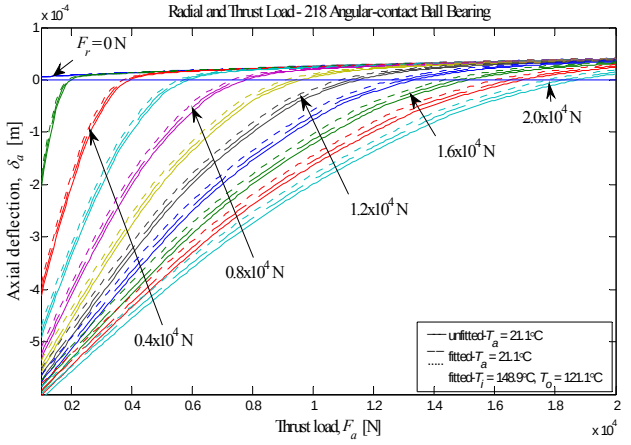

Fig. 15 Axial deflection, δ_a, as a function of the thrust load, F_a

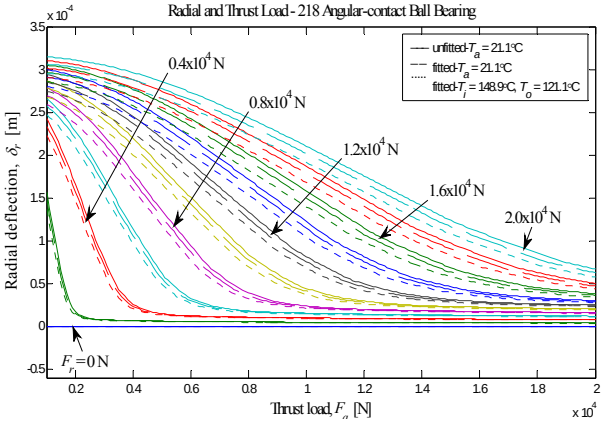

Fig. 16 Radial deflection, δ_r, as a function of the thrust load, F_a

References

[1] Stribeck, R. "Ball Bearings for Various Loads," *Trans. ASME* 29, 420-463, 1907.

[2] Sjoväll, H. "The Load Distribution within Ball and Roller Bearings under Given External Radial and Axial Load," *Teknisk Tidskrift,* Mek., h.9, 1933.

[3] Jones, A. *Analysis of Stresses and Deflections,* New Departure Engineering Data, Bristol, Conn., 1946.

[4] Rumbarger, J. "Thrust Bearings with Eccentric Loads," *Mach. Des.,* Feb. 15, 1962.

[5] Harris, T. Rolling Bearing Analysis, 4th ed., John Wiley & Sons Inc., New York, 2001.

[6] Ricci, M. C. *Internal loading distribution in statically loaded ball bearings subjected to a thrust load with variable eccentricity*, to be presented at DINCON'09 8th Brazilian Conference on Dynamics, Control and Applications, May, 18-22, Bauru, Brazil, 2009.

[7] Ricci, M. C. *Internal loading distribution in statically loaded ball bearings subjected to a combined radial and thrust load*, to be presented at 6th ICCSM International Congress of Croatian Society of Mechanics, Sept. 30 to Oct. 2, Dubrovnik, Croatia, 2009.

[8] Ricci, M. C. *Internal loading distribution in statically loaded ball bearings subjected to a combined radial, thrust, and moment load*, to be presented at 60th International Astronautical Congress, October, 12-16, Daejeon, South Korea, 2009.

[9] Hamrock, B. J. and Anderson, W. J. Arched-Outer-Race Ball-Bearing Considering Centrifugal Forces. NASA TN D-6765, 1972.

[10] Hertz, H. "On the contact of Rigid Elastic Solids and on Hardness," in *Miscellaneous Papers*, MacMillan, London. 163-183, 1896.

[11] Hamrock, B. J. and Anderson, W. J. Rolling-Element Bearings. NASA RP 1105, 1983.